Experimental Investigation of Stearic Acid in the Thermal Battery Comprising a Fin and Tube Heat Exchanger

Dinesh Kumar Saini
Mechanical Engineering Department, National Institute of Technology, Kurukshetra

Chandrashekara M
Mechanical Engineering Department, National Institute of Technology, Kurukshetra

https://doi.org/10.5109/6781068

出版情報：Evergreen. 10 (1), pp.170-181, 2023-03. 九州大学グリーンテクノロジー研究教育センター
バージョン：

Experimental Investigation of Stearic Acid in the Thermal Battery Comprising a Fin and Tube Heat Exchanger

Dinesh Kumar Saini[1,*], Chandrashekara M[2]

[1,2]Mechanical Engineering Department, National Institute of Technology, Kurukshetra, Haryana-136119, India

*Author to whom correspondence should be addressed:
E-mail: dinesh_62000005@nitkkr.ac.in

(Received December 17, 2022; Revised February 15, 2023; accepted February 22, 2023).

Abstract: Phase change materials (PCM) are employed in thermal energy storage (TES) systems for various applications due to their high energy density. This paper uses a fin and tube heat exchanger made of aluminium and copper in the thermal battery to enhance the heat transfer rate. The HYTHERM 600 is used as the heat transfer fluid (HTF), and stearic acid as the PCM. The experiment analyses the thermal behaviour of stearic acid in the thermal battery. The HTF maintains around 80°C and 85°C in the Hot HTF tank. Results show that conduction is dominant during the early melting stages; however, natural convection supersedes conduction after the stearic acid has liquefied. Conduction serves as the main mechanism of heat transfer during the discharging. The HTF temperature considerably enhances the stearic acid melting rate. The energy storage while charging and discharging is 248.03 kJ/kg and 211.81 kJ/kg, 254.50 kJ/kg, and 218.35 kJ/kg at 80°C and 85°C hot HTF temperatures. As the HTF temperature increases from 80°C to 85°C, the charging efficiency and higher temperature increase by 8.03% and 6.76%, and the melting time drops by 18.19% during the melting process, but in the discharging of stearic acid, discharging efficiency and lower temperature increases by 6.92% and 7.06%, and discharging time decreases by 25%.

Keywords: Thermal energy storage; Phase change materials; Stearic acid; Heat transfer fluid; Thermal battery

1. Introduction

Nowadays, it is believed that energy is a fundamental human need. It must be reliable, financially feasible, easily accessible in the long run, and environmentally friendly. Because of the rising demand for power and energy in our society, using non-renewable energy sources affects the environment. For this reason, it is necessary to concentrate on renewable energy sources (RES). India has a vast potential for RES utilisation. The most accessible RES found in nature is solar energy. Many uses of solar energy directly include water heating with solar water heaters and cooking with solar cookers. Since solar-powered appliances like water heaters and solar cookers can only work when sunlight is present, solar thermal energy storage (TES) systems are necessary. TES is a well-established technology that has been included in energy systems to cope with the instant rise in energy demand and decrease energy costs through effective and sustainable integration. TES improves energy management in various thermal sectors[1)]. The following articles described energy management strategies related to several sectors [2–7)]. Materials are used in TES systems to store energy as latent heat (LH), sensible heat (SH), and thermochemical. Latent heat storage (LHS) materials store/release energy due to changes in phase nearly at a constant temperature, whereas SH storage materials store/release energy due to an increase/decrease in temperature without changing phase. The materials store or release energy through a reversible chemical reaction in thermochemical energy storage. Due to the requirement for a sizable amount of material in the SH storage system, solid-liquid LH storage materials are used most frequently [8)].

PCMs are another name for LH storage materials. PCMs can be classified as organic, inorganic, and eutectic. When a phase transition (melting and solidification) occurs, PCMs have a higher storage density than SH storage materials because they can store the energy in the smallest possible area. Numerous researchers investigated the heat exchanger design used to transmit heat inside the LHS unit for various applications and the thermophysical characteristics of PCMs[9,10)]. Several experimental research studies have been done to analyse the PCM behaviour and use them in the TES system for different applications [11–16)]. In recent years, PCM has received a lot of attention. Lower thermal conductivity is the primary disadvantage of the PCM, which reduces system efficiency and raises the charging and discharging time. Several studies have been conducted to improve thermal

conductivity, heat transfer, and heat distribution inside the LHS unit to melt and solidify the PCM easily. Some of these are discussed below[17,18].

The main problem that prevents heat transfer is PCM's low thermal conductivity. In the liquid phase, convection can improve heat transmission, but it is not sufficient to resolve the issue in the solid phase due to the absence of convection. Hence, PCM is upgraded to a material with increased thermal conductivity to meet the process's requirement for faster heat transfer. However, convection in the liquid phase is reduced or eliminated by adding materials with higher thermal conductivity. The charging time decreases by 60% and improves the useful heat gains by using aluminium powder of 80 μm with 0.5 mass fraction in paraffin wax[19]. Byrne et al.[20] used a mixture of fatty acids as PCM embedded in expanded graphite to examine the thermal performance and utilised it for energy storage. Gunjo et al.[21] examined the thermal behaviour of Paraffin with 4% CuO nanoparticles. They observed that density, viscosity, thermal conductivity, charging rate and discharging rate increased by 29%, 18.3%, 55%, 1.7 and 1.8 times, respectively. Karimi et al.[22] analysed Paraffin C18 to increase the melting and discharging rate by using a helical coil and porous metal foam in the LHS unit. The outcomes show that a porous medium can significantly decrease the charging/discharging time by 57%, depending on the intake of HTF. Raising the HTF flow rate may slightly shorten the charging time, but porous media has a more significant impact. A lower HTF flow rate increases the discharge rate and reduces the solidification time.

A suitable heat exchanger is necessary to analyse PCM's thermal performance (melting and solidification). The heat transfer inside the LHS unit heavily depends on the heat exchange design to investigate the PCM performance. A pipe model and a horizontal shell and tube model were analysed by Agyenim et al.[23] using temperature-time curves and isothermal contour plots. They found that the conductive heat transfer in the shell and tube model was less critical than the convective heat transfer in the pipe model. The outcomes show that the temperature gradients for both systems were 2.5% and 3.5% higher in the axial direction than the radial direction during the phase change. An experimental investigation was performed by Zhang et al.[24] to examine the performance of Paraffin in a vertical LHS unit with a snowflake fin design. The longitudinal fin improves the snowflake fin design in terms of charging and discharging time, decreasing by 32.23% and 51.81%, respectively. Additionally, they observed that the snowflake fin surpasses the conventional longitudinal fin for the discharging process since water's HTF (heat transfer factor) increases by 12.27% for melting and 179.81% for solidification.

Lacroix[25] evaluated the PCM behaviour in a shell and tube LHS unit through a numerical model. The results exhibited that the optimum working conditions for annular fins are low inlet temperatures and moderate mass flow rates. Punniakodi and Senthil[26] used a modified heat transfer tube to examine the PCM melting inside a vertical container. They stated that the intake temperature of HTF is an important factor for melting the PCM. During the LHS unit analysis, Paraffin acts as the PCM, water as the HTF, and HTF travels circumferentially via the outer tube in a downward direction. The heat transfer improves during the melting and solidification of PCM in an LHS unit comprising the cylindrical vertical tube with longitudinal fins. The V-shaped fin arrangement leads to the best outcomes[27]. An experiment was performed by Murthy et al.[28] to utilise shellac wax for solar TES systems. They discussed the effect of natural convection and the advancement of the melting and solidification front. The charging rate noticeably improves, and the melting time decreases when the HTF flow rate increases. The increased flow rate during the discharge operation has minimal impact on the discharge efficiency.

Liu and Groulx[29] used a central copper pipe with fins along the container length to investigate heat transfer within a cylindrical LHS system throughout the melting and solidification processes. The outcomes indicate that conduction is crucial during the initial melting stages, but natural convection regulates heat transmission once enough liquid PCM melts in the container. Conduction controls the entire solidification process. The HTF input temperature considerably affects the total melting time, but the HTF flow rates have little influence. Similarly, Kothari et al. [1] analysed the heat transfer rate of Paraffin wax inside an annulus of the LHS unit. A copper pipe with longitudinal fins passes along the cylindrical LHS unit length to observe the thermal performance of Paraffin wax.

Rathod and Banerjee[30] demonstrated that the flow rate is not as significantly affected by the HTF inlet temperature as the melt fraction. The results of the experiments show that PCM’s total melting time rises when the HTF's mass flow rate and inlet temperature decrease. Additionally, they found that the improvement in heat transfer is more sensitive to a rise in HTF intake temperature than HTF mass flow rate. Adding three longitudinal fins to the HTF tube can reduce the solidification time by as much as 43.6%[31]. The overall melting time of PCM packed in three LHS units, rectangular, cylindrical, and cylindrical shells, each with the same volume and heat transmission surface area, was compared by Vyshak and Jilani [32]. They found that cylindrical shell containers store the same energy in the minimum time for the same PCM mass and heat transfer surface area. With higher PCM mass, the geometric effect is more noticeable.

The melting front appeared at various points close to the HTF tube, and it advanced toward the shell at different rates, according to the outcomes of the investigation of the impact of raising the HTF's intake temperature during the PCM melting operation. The total charging time decreases by 37% as the inlet water temperature reaches 80 °C[33]. A 1-D model based on the enthalpy method was used by Silva et al. [34] to execute a numerical analysis of paraffin

wax in the vertical rectangular LHS unit. During the melting and solidification operations, one of the walls is continuously heated while an airflow stream cools the other wall. The results demonstrate that a basic numerical model may reasonably predict the performance of the rectangular LHS unit.

Khan and khan[35,36] experimentally analysed the charging performance of Paraffin in a shell and tube LHS unit comprising longitudinal fins. They observed that as the intake HTF temperature raised from 52 °C to 67 °C, the state-changing rate and power improved by 50.08% and 69.71%. The HTF volume flow rate effect is relatively less but diminishes as HTF intake temperature rises. The LHS unit comprised of a multi-tube model significantly improved the average melting and solidification powers by 75.53% and 27.04% as there was a rise in the temperature difference between PCM and intake fluid from 52 °C to 62 °C and 15 °C to 5 °C respectively.

Zivkovic and Fujii[37] conducted a numerical investigation of a PCM charging time inside a rectangular and cylindrical LHS unit. They found that the rectangular LHS unit melts nearly half as long as the cylindrical LHS unit for the same volume and heat transmission area. Biwole et al.[38] optimised the number, size, and position of fins in the container by conducting a numerical heat transfer analysis inside a rectangular enclosure. According to the results, adding additional fins enhances SHS and LHS in the PCM and lowers the stabilisation temperature and front plate stabilisation time during phase transition.

To examine the thermal performance of PCM, many researchers used various heat exchanger models with fins in the cylindrical LHS units[1,17,22–24,26,28–31,35,36]. Thus, it can be concluded from the literature that few researchers used heat exchangers with fins in the rectangular LHS unit [34,37,38]. Additionally, it is noted that a significant portion of the literature is based on numerical analysis [16,18,25,32,38,39], lacking experimental analysis of PCM in the proposed rectangular LHS unit with fin and tube type heat exchanger.

The present paper focuses on an experimental investigation of stearic acid (PCM) in a rectangular Thermal battery comprising a fin and tube-type heat exchangers with aluminium fins and copper tubes. This heat exchanger improves the heat transfer and distribution inside the thermal battery. In this paper, Stearic acid's thermal performance (melting and solidification) is experimentally analysed during phase change heat transfer throughout both processes in a rectangular thermal battery. The impact of hot HTF temperature on the charging and discharging of stearic acid has been studied.

2. Methodology

2.1 Phase Change Material

Due to their advantageous characteristics, such as non-toxicity, high latent heat, non-corrosiveness, affordability, chemical and thermal stability over the appropriate temperature range, organic PCMs are most frequently utilised in low-temperature thermal applications. Stearic acid is a well-known organic PCM used in air and water heating applications. Stearic acid is selected as a PCM for the current analysis. BRM chemicals provided the commercial-grade stearic acid having the thermophysical properties stated in Table 1.

Table 1. Thermophysical characteristics of stearic acid.[15]

Parameters	**Values**	
IUPAC name	Octadecanoic acid	
Chemical formula	$C_{18}H_{36}O_2$	
Appearance	White powder	
Molecular weight	284.5 g/mol	
Thermal conductivity (W/mK)	0.172	
Melting temperature (°C)	55	
Boiling temperature (°C)	381	
Density (kg/m^3)	Solid	965
	liquid	848
Enthalpy of fusion (kJ/kg)	160	
Specific heat (kJ/kg.K)	Solid	1.6
	liquid	2.2

2.2 Experimental Setup

Fig. 1 depicts the schematic diagram of the experimental setup. It comprises a thermal battery, temperature sensors, a scanner, a magnetic gear pump, hot/cold HTF tanks, and connecting pipes. Connecting pipes connect all the parts, and Fig. 2 shows a real lab-scale pictorial diagram of the entire experimental setup.

2.2.1 Thermal battery

Thermal battery is the critical component of the experimental setup investigating stearic acid behavior. Fig. 3 displays the dimension specifications and an actual pictorial diagram of the lab-scale thermal battery. Arc welding is used to construct this battery from a 14 gauge (0.2 cm) thick mild steel sheet. This battery is 34 cm long, 9 cm wide, and 32 cm high. A fin and tube heat exchanger is placed in the centre to uniformly transfer heat from HTF to stearic acid in all directions. Copper tubes of 1 cm diameter and 0.1 cm aluminium fins make the heat exchanger. Heat transfer is made more likely by the aluminum fins over the copper tubes. A 2 cm wide space is left at the sides, top, and bottom of the battery for the stearic acid. The HTF enters the thermal battery from the bottom and exits from the top. The thermocouples (T1 and T2) and (T3 and T4) are inserted at 1 cm and 27 cm height inside the thermal battery, respectively.

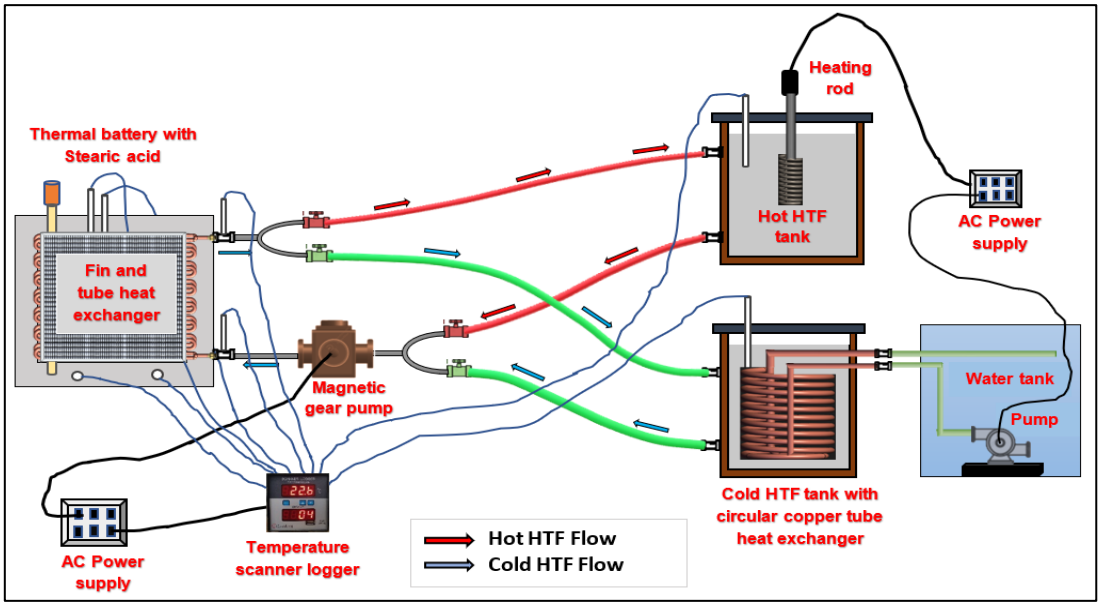

Fig. 1: Schematic diagram of a complete experimental setup

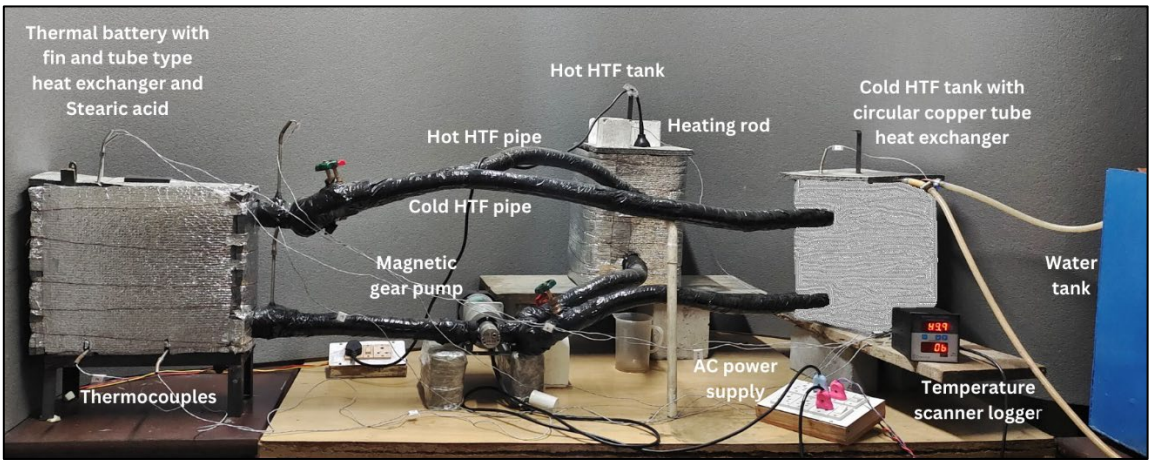

Fig. 2: Real lab-scale pictorial diagram of an experimental setup

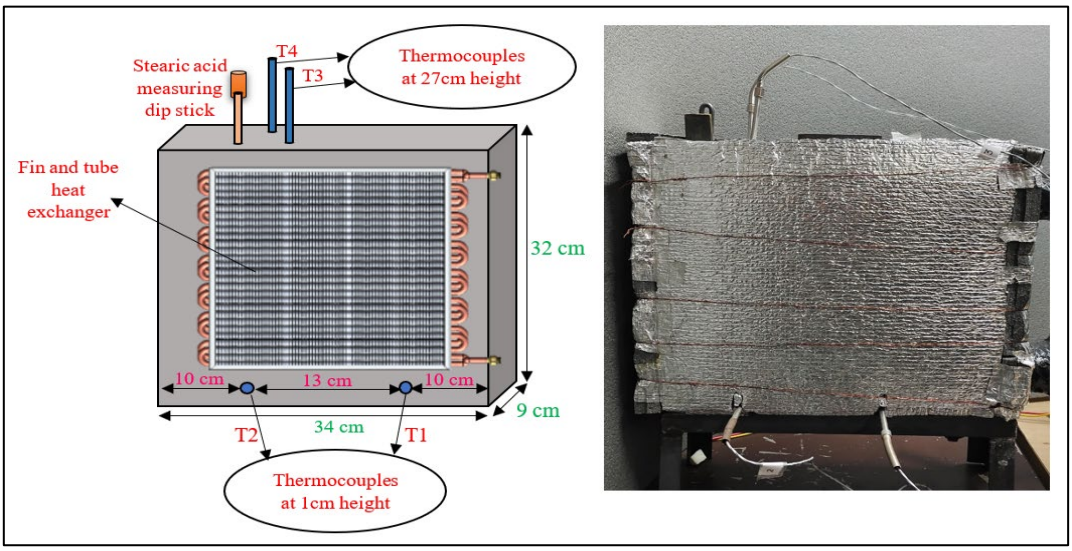

Fig. 3: Dimension specifications and an actual pictorial diagram of the lab-scale thermal battery

2.2.2 Temperature sensors and temperature scanner logger

The HTF and stearic acid temperatures have been measured at various locations inside the thermal battery using a three-wire, ultra-precise RTD PT-100 temperature sensor. The temperature range for these sensors is -100 to 600°C. The temperature sensors are connected to a Countron data logger with a temperature indicator scanner acting as the display unit. The temperature is recorded at every location in the experimental setup according to the date, time, and selected channels. The resolution and accuracy of these sensors are 0.1°C and ±0.1°C ±1 least significant digit.

2.2.3 Magnetic gear pump

The HTF is pumped from the HTF tank to the thermal battery for the melting/discharging of stearic acid using a high-temperature magnetic gear pump linked with an induction motor made by an oriental motor. This pump helps to flow the HTF at a constant mass flow rate of 6 LPM throughout the cycle, irrespective of the length of connected pipes. The 150 W induction motor has 2650 revolutions per minute.

2.2.4 Heat transfer fluid

HYTHERM 600 is employed as the HTF for the melting and solidification of stearic acid. This HTF allows for high-temperature heat transfers up to 320°C. Due to the following properties in Table 2, this HTF is considered suitable for charging/discharging stearic acid.

Table 2. Thermophysical Properties of HYTHERM 600 [40)]

Parameters	Value
Specific heat (kJ/kg K)	2.19
Specific gravity	0.825
Viscosity index	100
Appearance	Clear and bright
Maximum film temp. (°C)	345
Pour point temp. (°C)	−45
Flashpoint temp. (°C)	220
Auto-ignition temp. (°C)	426

2.2.5 Hot/Cold HTF Tank

The Hot HTF tank transfers the HTF to the thermal battery to melt the stearic acid. It contains 10 litres of HTF, heated to the required temperature by a 1.5 kW heating rod. The tank is well insulated with a Polyurethane Foam sheet of 2 cm thickness to avoid heat loss to the environment. The thermal battery receives HTF from the cold HTF tank via a magnetic gear pump to discharge the stearic acid. 13 litres of HTF are stored in this tank. The HTF absorbs the heat from the stearic acid and continuously cools it with fresh water.

2.2.6 Connecting pipes

The hot/cold HTF tank and the thermal battery are connected to the magnetic gear pump via flexible stainless steel (SS) 304 pipes. All the connecting pipes have a 1.5 cm internal diameter, and hexagonal bolts are press-fitted into the ends to connect the pipes. The thermal battery receives HTF from the HTF tank via a closed circuit formed by these pipes. These pipes can bear temperatures from -20°C to 400°C and provide enough insulation to prevent heat loss to the environment.

2.3 Experimental procedure

Firstly, stearic acid is heated in the tank to a temperature of 80°C before being poured into a thermal battery for analysis. Because of the density difference between stearic acid's solid and liquid phases, a gap is left at the top when the thermal battery is filled. During the analysis, two processes -charging and discharging take place inside the thermal battery. Firstly, the circulation of cold HTF is done inside the pipes to make sure that the temperature displayed by each thermocouple in the display unit is the same. After that, perform the charging and discharging cycle using the experimental setup.

2.3.1 Charging/Melting of stearic acid

Heat the HTF to the desired temperature, then open the two-way valve to allow the hot HTF to circulate throughout the system at a constant flow rate of 6 LPM. The hot HTF enters the heat exchanger inside the thermal battery and transfers the heat to the stearic acid. The thermocouples start recording temperature when the stearic acid begins to melt. This process continues inside the thermal battery until the steady state temperature is attained. For analysis, the HTF is maintained at 80 °C and 85 °C in a hot HTF tank.

2.3.2 Discharging/Solidification of stearic acid

In this procedure, the stearic acid is discharged by the flow of cold HTF within the heat exchanger inside the thermal battery. The HTF absorbs the heat from the hot stearic acid and transfers it to the cold HTF tank. Fresh water is used to cool this HTF inside the tank. This procedure continues until the battery's top and bottom attains steady state temperature.

2.4 Experimental data analysis

2.4.1 Charging Process

The control volume of the thermal battery is used to analyse the thermal performance of stearic acid. The HTF temperature at the entry and exit of the thermal battery was measured after a time interval of one minute. Stearic acid's instantaneous thermal power gained during the charging process is added to determine the total thermal power. The instantaneous and total thermal power transfer from the HTF to the stearic acid during the melting process is shown in Eq. 1 and Eq. 2. The actual energy stored by stearic acid during the charging operation is

shown in Eq. 3. The ratio of actual energy stored in the stearic acid to the energy transferred by heated HTF to the stearic acid is known as the charging efficiency and is expressed in Eq. 4.[28)]

$$q_c = \dot{m}_{HTF} * c_{p,HTF} * \left(T_{HTF,in} - T_{HTF,ex}\right) \quad (1)$$

$$Q_c = \sum_{i=1}^{n} q_c * \Delta t \quad (2)$$

$$Q_{SA,c} = m_{SA}\{c_{p,s}(T_m - T_i) + L_{SA} + c_{p,l}(T_f - T_m)\} \quad (3)$$

$$\eta_c = \frac{Q_{SA,c}}{Q_c} \quad (4)$$

2.4.2. Discharging Process

The HTF's instantaneous and total thermal power gained by HTF from the stearic acid during the discharging process is expressed in Eq. 5 and Eq. 6. The actual energy discharged by stearic acid during the discharging process is given in Eq. 7. The ratio of the energy gained by cold HTF to the energy released by stearic acid is called the discharging efficiency and is expressed in Eq. 8.[28)]

$$q_D = \dot{m}_{HTF} * c_{p,HTF} * \left(T_{HTF,ex} - T_{HTF,in}\right) \quad (5)$$

$$Q_D = \sum_{i=1}^{n} q_D * \Delta t \quad (6)$$

$$Q_{SA,D} = m_{SA}\{c_{p,l}(T_i - T_m) + L_{SA} + c_{p,s}(T_m - T_f)\} \quad (7)$$

$$\eta_c = \frac{Q_D}{Q_{SA,D}} \quad (8)$$

3. Results and discussion

This research article has conducted two experimental trials with HTF temperatures of 80°C and 85°C and a set mass flow rate of 6 LPM to analyse stearic acid inside the thermal battery.

3.1 Stearic acid investigation at 80 ºC hot HTF in the tank

3.1.1 Melting/charging of stearic acid

The temperature change of HTF at the thermal battery's entry and exit points and inside the hot HTF tank is shown in Fig. 4. The HTF heats up inside the hot HTF tank through the heating rod and maintains a temperature of about 80ºC during the charging process. This temperature is reached after 16 minutes by the 1.5 kW heating rod. There is a more noticeable HTF temperature difference between the entry and exit points of the thermal battery during the earlier melting stages. Due to this, the stearic acid close to the fins absorbs heat very quickly from the hot HTF in the earlier charging stages and accelerates the melting rate.

Fig. 5 depicts the temporal variation in stearic acid temperature (T1 and T2 at 1 cm height) and (T3 and T4 at 27 cm height) from the base of the thermal battery. The curve illustrates that the temperature at T1 first reaches the melting point, followed by T2 in the sequence. The melting front moves from T1 to T2 because T1 is close to the HTF entry, and T2 is farther from the HTF entry. This is because the HTF and stearic acid have a tremendous temperature difference nearer the entry point. As HTF moves forward, the temperature difference drops, decreasing the heat transfer rate.

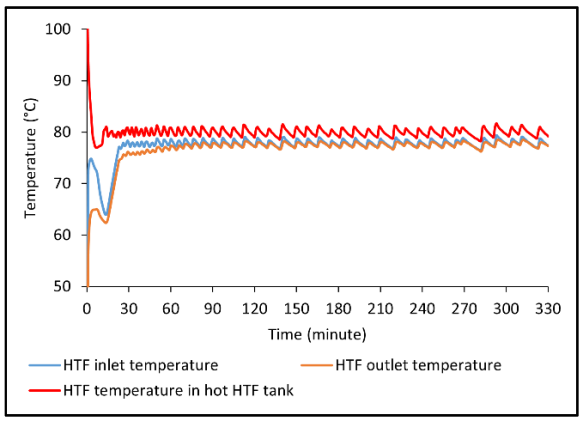

Fig. 4: HTF temperature at the thermal battery's entry and exit and in the hot HTF tank at 80 °C

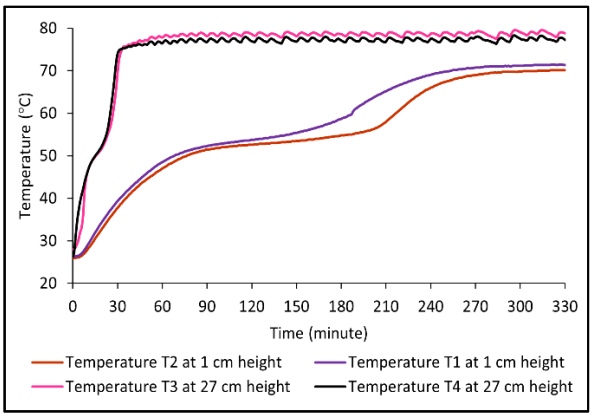

Fig. 5: Temperatures at different thermal battery heights for 80°C hot HTF in the tank during the charging process

The heat exchanger improves the heat transfer rate and maintains the uniform heat distribution inside the thermal battery. The temperature of the fins rises continuously during the initial phase, indicating that most heat transmission occurs via conduction within the solid stearic acid. As a result, the stearic acid inside and around the heat exchanger melts first. After that, the stearic acid next to the heat exchanger melts, and the melting front moves from the heat exchanger fins to the walls of the thermal battery. Further, Stearic acid exists in liquid and solid forms inside the battery. Due to the density difference, the liquid form of stearic acid rises upward and interacts with the surrounding solid stearic acid, accelerating the melting rate as the charging process proceeds. Heat transmission by convection causes the liquid stearic acid to move in an upward direction. Afterwards, the stearic acid experiences heat transmission through conduction and convection modes inside the thermal battery. Because of this, stearic

acid at 27 cm thermal battery height melts before that at 1 cm height and achieves a higher temperature. On the top side (27 cm height), Stearic acid at the location T3 melts first, followed by T4. Hence, the stearic acid melting front spreads from top to bottom inside the thermal battery.

The average temperature variation of the stearic acid inside the thermal battery is depicted over time in Fig. 6. The average temperature of stearic acid at the thermal battery's 27cm and 1 cm height takes 40 minutes and 330 minutes to reach a steady state, respectively. Because the stearic acid has low thermal conductivity and the heat transfer occurs mainly by convection, the stearic acid inside the rectangular thermal battery requires at least 330 minutes to achieve a steady state of 74ºC during the melting process. Conduction heat transmission takes place when melting is still in its early stages. Later, the stearic acid inside the thermal battery melts by conduction and convection modes of heat transfer.

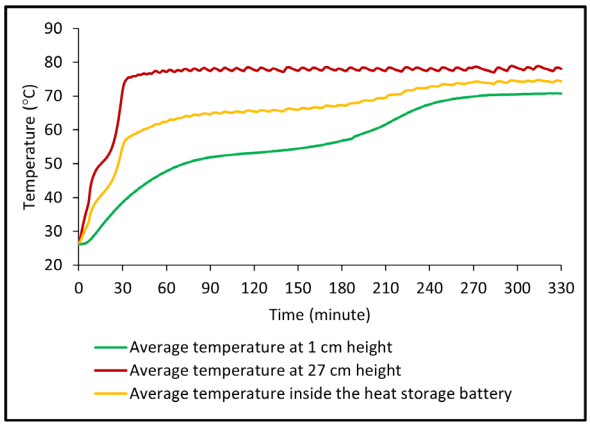

Fig. 6: Average temperature inside the thermal battery for 80°C hot HTF in the tank during the charging process

3.1.2 Discharging/Solidification of Stearic acid

The heat stored by Stearic acid during the charging operation is used in many applications like water and air heating via discharging operation. Stearic acid solidifies with the HTF at 25ºC in the cold HTF tank. The HTF circulates between the high-temperature source (stearic acid) and the low-temperature sink (water) at a constant mass flow rate of 6 LPM in the experimental setup. The water circulates inside the circular copper tube heat exchanger placed in the HTF tank. Natural convection and radiation help to reject more heat from the HTF to the surrounding and keep the HTF at a low temperature as the tank is not insulated. The variation of stearic acid temperature at different locations inside the thermal battery throughout the discharging process is shown in Fig. 7. Stearic acid has a high temperature and low density at the top of the thermal battery. The curve indicates that the stearic acid at 27 cm height (T3 and T4) cools more rapidly than the 1 cm height (T1 and T2) inside the thermal battery due to convection, conduction and more significant temperature differences between the stearic acid and cold HTF in the initial discharging stages. Therefore, the discharging front moves from top to bottom. The thermocouples T3 and T4 are located at 27cm height on both sides of the heat exchanger, giving different discharging curves. After some time, conduction plays a vital role in transferring the heat from the solid stearic acid to the cold HTF during the discharging operation. The heat transfer rate and temperature gradient decrease as a solid stearic acid layer develops on the heat exchanger's fins over time. Therefore, the heat transferred mainly occurs through the conduction in the whole discharging operation.

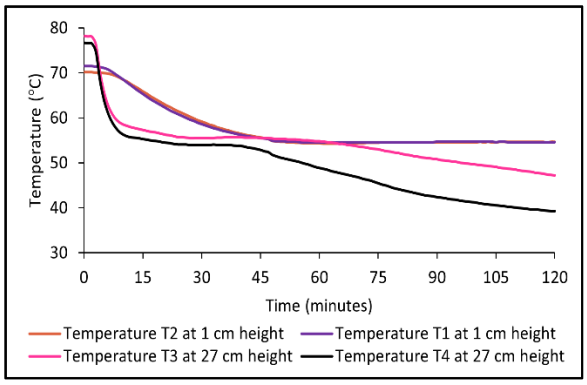

Fig. 7: Temperatures at different thermal battery heights for 80°C hot HTF in the tank during the discharging process

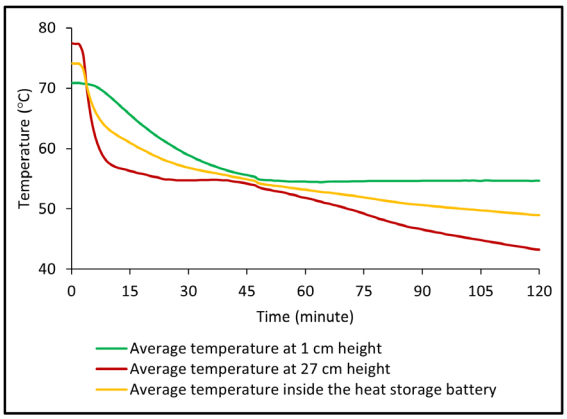

Fig. 8: Average temperature inside the thermal battery for 80ºC hot HTF in the tank during discharging process

Fig. 8 shows the temporal variation of the average temperature of the stearic acid inside the thermal battery during the discharging operation. Within 2 hours, the average temperature at the 72 cm height reaches 77.35ºC to 43.25ºC, and at 1 cm height goes 70.85ºC to 54.65ºC. In the thermal battery, stearic acid typically reaches a temperature of 48.9ºC from 74ºC. The heat extracted by HTF from stearic acid is used for various purposes, including water and space heating.

3.2 Stearic acid investigation at 85 ºC hot HTF in the tank

3.2.1 Charging/Melting of Stearic acid

The timewise variation of HTF temperature at the entry and exit points of the thermal battery and in the hot HTF tank is depicted in Fig. 9, similar to the prior case. A

temperature of nearly 85ºC is maintained in the hot HTF tank with the help of a 1.5 kW heating rod. The HTF achieves this temperature within 18 minutes. The difference between the HTF temperature at the entrance and exit point is more noticeable, and the stearic acid adjacent to the fins absorbs heat quickly during the initial charging stages. The temperature of stearic acid changes over time at the different locations inside the thermal battery, as shown in Fig. 10. Because HTF delivers to the thermal battery at a greater temperature than in the prior case, the stearic acid reaches a steady state temperature more quickly. The thermal battery's internal heat transfer mechanism is similar to that previous case.

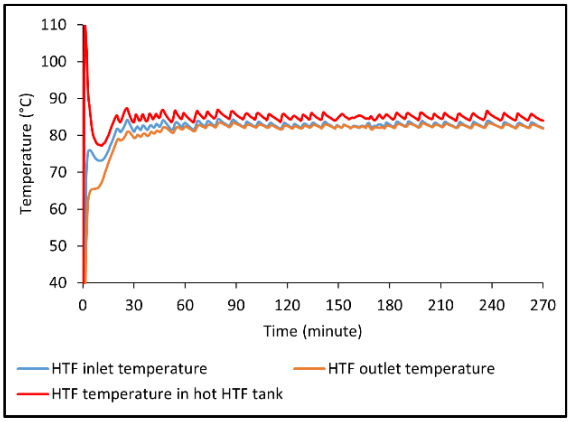

Fig. 9: HTF temperature at the thermal battery's entry and exit and in the hot HTF tank at 85°C

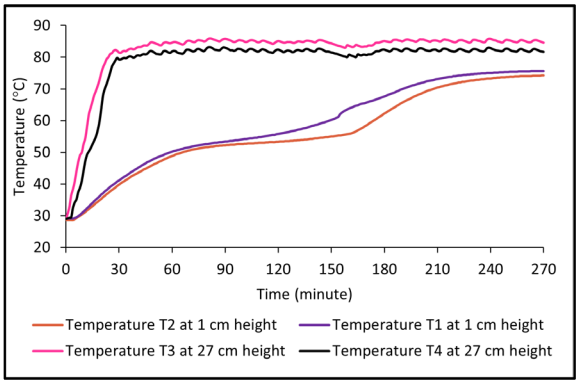

Fig. 10: Temperature at different thermal battery heights for 85°C hot HTF in the tank during the charging process

Fig. 11 illustrates the temporal variation of the average stearic acid temperature inside the thermal battery. The average temperature of stearic acid at the 27 cm height (T3 and T4) reaches a steady state temperature of 83.12ºC in 50 minutes. Stearic acid at 1 cm height takes 270 minutes to achieve a 74.9ºC steady state temperature. Hence, the thermal battery takes at least 270 minutes to melt the stearic acid and reach a steady state average temperature of 79ºC. As a result, when the HTF temperature is higher, the rectangular thermal battery charges more quickly.

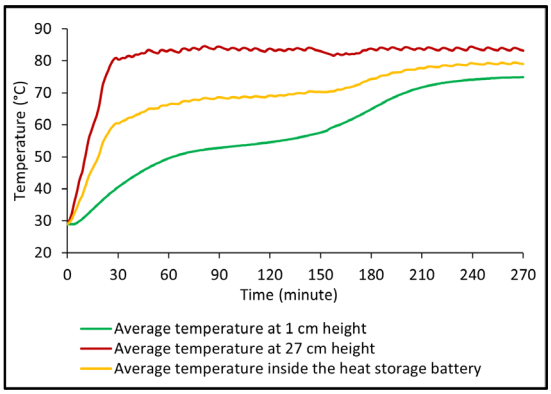

Fig. 11: Average temperature inside the thermal battery for 85°C hot HTF in the tank during the charging process

3.2.2 Discharging/Solidification of Stearic acid

Like the previous case, cold HTF is used to discharge/solidify the stearic acid inside the thermal battery. The stearic acid's temperature variation over time at different heights is shown in Fig. 12. Due to the high temperature and low density of stearic acid at the top of the thermal battery, convection and conduction heat transfer occur during the initial discharging stages. Stearic acid at 27 cm height solidifies more rapidly than the 1 cm height. Afterwards, conduction heat transfer occurs between the solid stearic acid and cold HTF. Due to a solid stearic acid layer that accumulates with time on the heat exchanger's fins, the heat transmission and temperature gradient gradually decrease.

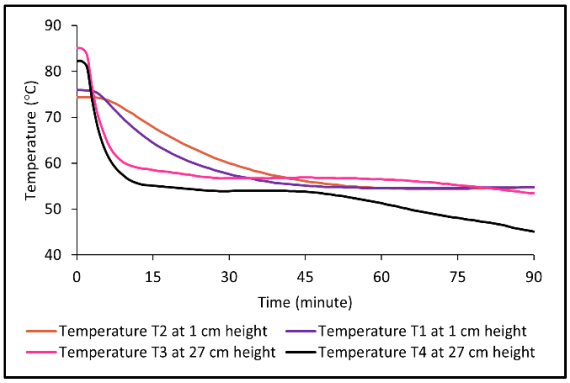

Fig. 12: Temperature at different thermal battery heights for 85°C hot HTF in the tank during the discharging process

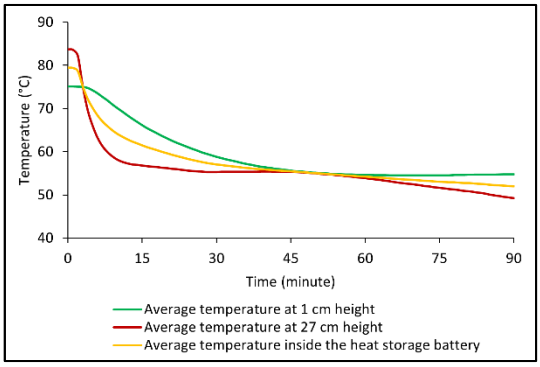

Fig.13: Average temperature inside the thermal battery for 85ºC hot HTF in the tank during discharging process

Fig. 13 depicts the variation of the average temperature of stearic acid at the different heights of the battery. The stearic acid at 27 cm height reaches 49.55ºC, and at 1 cm height reaches 54.75ºC in 90 minutes. Stearic acid usually reaches a temperature of 52.35ºC in a thermal battery after 90 minutes.

3.3 Performance comparison of Stearic acid

The temperature variation of stearic acid during charging (heat storage) and discharging (heat release) at HTF temperatures of 80ºC and 85ºC in the hot HTF tank is shown in Fig. 14. The figure compares the performance of stearic acid in both cases and found that the stearic acid melts more quickly from the heated HTF at 85ºC than at 80ºC. When the temperature is high, the HTF can carry more heat, transfer heat to the stearic acid faster and achieve a higher steady-state temperature in less time during both processes. The highest temperature of stearic acid experimentally reaches 74ºC and 79ºC in 330 minutes and 270 minutes during the melting process, while the hot HTF is at 80ºC and 85ºC in the hot HTF tank, respectively. The stearic acid reaches 48.9ºC and 52.35ºC in 120 minutes and 90 minutes during the discharging process. As the hot HTF temperature in the tank rises from 80ºC to 85ºC while charging the stearic acid, the melting time drops by 18.19%, and the higher temperature increases by 6.76%. In the discharging of stearic acid, discharging time decreases by 25%, and the lower temperature increases by 7.06%.

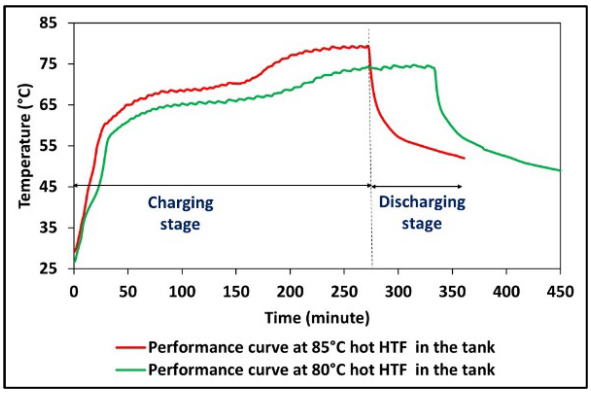

Fig. 14: Charging (heat storage) and Discharging (heat release) performance curve of stearic acid at 80ºC and 85ºC hot HTF in the hot HTF tank

Table 3. Charging and discharging efficiency of stearic acid when the hot HTF in the tank at 80 ºC and 85ºC

	Hot HTF temperature	Stearic acid temperature (ºC)			$Q_{SA,C}$ (kJ)	Q_C (kJ)	η_C (%)
Charging		$T_{avg.}$	T_i	T_f			
	80ºC	65.71	26.63	74.38	1636.98	3990.29	41.02
	85ºC	68.95	28.95	79.01	1679.71	3790.18	44.32
Discharging	**Hot HTF temperature**	Stearic acid temperature (ºC)			$Q_{SA,D}$ (kJ)	Q_D (KJ)	η_D (%)
		$T_{avg.}$	T_i	T_f			
	80ºC	54.81	74.15	48.95	1397.95	902.85	64.58
	85ºC	57.54	79.43	52.12	1441.14	995.12	69.05

3.4 Charging and Discharging efficiency of stearic acid

When the HTF heats at 80ºC and 85ºC, Table 3 summarises the stearic acid's initial, final, and average temperatures and the charging and discharging efficiencies. The charging and discharging efficiencies are 41.02 % and 64.58 %, 44.32 % and 69.05 % for the 80ºC and 85ºC hot HTF temperatures, respectively. When the HTF heats to 85ºC rather than 80ºC, the charging and discharging efficiencies increase by 8.03 % and 6.92 %, respectively. The energy storage while charging and discharging is 248.03 kJ/kg and 211.81 kJ/kg, 254.50 and 218.35 kJ/kg at 80ºC and 85ºC hot HTF temperatures.

As a result, stearic acid in the rectangular vertical thermal battery can be melted more quickly and effectively at greater temperatures. Hence, energy storage efficiency increases with HTF temperature, and faster charging/melting times are crucial for improving the rectangular thermal battery's performance.

4. Conclusions

PCMs-based TES systems are becoming more prevalent due to excellent energy efficiency, economic viability, and simplicity of integration with renewable resources. PCMs are suitable for various applications due to its high energy density. An experimental investigation of stearic acid's thermal performance inside the vertical thermal battery has been done in this paper. The conclusions from the present work are

- During charging inside the thermal battery, the stearic acid melts more quickly at the top than at the bottom.
- The fin and tube heat exchanger improves the heat transfer rate and distribution, and the heat transfer by conduction and natural convection mode usually occurs in the melting process.
- Heat conduction plays a critical role in solidification, Natural convection improves heat transfer during

heat storage, and HTF temperature strongly influences the charging and discharging rate.

- When the HTF inside the tank is 80ºC and 85ºC, respectively, the thermal battery needs a minimum of 330 minutes and 270 minutes to melt the stearic acid.
- As the hot HTF temperature in the tank rises from 80ºC to 85ºC while charging the stearic acid, the melting time drops by 18.19%, and the higher temperature increases by 6.76%. In the discharging of stearic acid, discharging time decreases by 25%, and the lower temperature increases by 7.06%.
- The charging and discharging efficiencies are 41.02% and 64.58%, 44.32% and 69.05% for the 80ºC and 85ºC hot HTF temperatures, respectively.
- When the HTF heats to 85ºC rather than 80ºC, the charging and discharging efficiencies increase by 8.03% and 6.92%, respectively.
- The energy storage while charging and discharging is 248.03 kJ/kg and 211.81 kJ/kg, 254.50 kJ/kg, and 218.35 kJ/kg at 80ºC and 85ºC hot HTF temperatures.
- The further scope of the work is to develop highly efficient thermal storage materials for various applications.

Nomenclature

TES	thermal energy storage (-)
LH	latent heat (kJ)
LHS	latent heat storage (-)
PCM	Phase change material (-)
SH	sensible heat (kJ)
L	latent heat of fusion (kJ kg^{-1})
q	instantaneous thermal power (W)
Q	total thermal power (kJ)
m	mass (kg)
$\dot{m}$	mass flow rate (kg s^{-1})
T	temperature (ºC)
t	time (s)
c_p	specific heat capacity (kJ kg^{-1} ºC $^{-1}$)

Greek symbols

Δ	difference (–)
η	efficiency (–)

Subscripts

HTF	heat transfer fluid
SA	stearic acid
s	solid
l	liquid
m	melting
i	initial
f	final
C	charging
D	discharging
in	inlet
ex	exit
avg.	average

References

1) R. Kothari, A. Ahmad, S. Kumar Chaurasia, and O. Prakash, "Experimental analysis of the heat transfer rate of phase change material inside a horizontal cylindrical latent heat energy storage system," *Mater Sci Energy Technol*, **5** 208–216 (2022). doi:10.1016/j.mset.2022.02.004.
2) M.K. Barai, and B.B. Saha, "Energy security and sustainability in japan," Evergreen, 2 (1) 49–56 (2015). doi:10.5109/1500427.
3) Y.D. Kim, K. Thu, and K.C. Ng, "Evaluation and parametric optimisation of the thermal performance and cost effectiveness of active-indirect solar hot water plants," Evergreen, 2 (2) 50–60 (2015). doi:10.5109/1544080.
4) H. Gima, and T. Yoshitake, "A comparative study of energy security in okinawa prefecture and the state of hawaii," Evergreen, 3 (2) 36–44 (2016). doi:10.5109/1800870.
5) M.I. Alhamid, N. Nasruddin, Budihardjo, E. Susanto, T.F. Vickary, and M. Arif Budiyanto, "Refrigeration cycle exergy-based analysis of hydrocarbon (r600a) refrigerant for optimisation of household refrigerator," Evergreen, 6 (1) 71–77 (2019). doi:10.5109/2321015.
6) N. Hamzah, M.F.M. Yasin, M.Z.M. Yusop, M.T. Zainal, and M.A.F. Rosli, "Identification of cnt growth region and optimum time for catalyst oxidation: experimental and modelling studies of flame synthesis," Evergreen, 6 (1) 85–91 (2019). doi:10.5109/2328409.
7) S.A. Shaedi, N. Mohd-Ghazali, J.T. Oh, R. Ahmad, and Y. Mohd-Yunos, "Entropy generation minimisation of two-phase flow in a mini channel with genetic algorithm," Evergreen, 6 (1) 39–43 (2019). doi:10.5109/2321004.
8) A. Sharma, V. v. Tyagi, C.R. Chen, and D. Buddhi, "Review on thermal energy storage with phase change materials and applications," Renewable and Sustainable Energy Reviews, 13 (2) 318–345 (2009). doi:10.1016/J.RSER.2007.10.005.
9) B. Zalba, J.M. Marín, L.F. Cabeza, and H. Mehling, "Review on thermal energy storage with phase change: materials, heat transfer analysis and applications," Appl Therm Eng, 23 (3) 251–283 (2003). doi:10.1016/S1359-4311(02)00192-8.
10) R.K. Sharma, P. Ganesan, and V. v Tyagi, "Long-term thermal and chemical reliability study of different organic phase change materials for thermal energy storage applications," J Therm Anal Calorim, 124 (3) 1357–1366 (2016). doi:10.1007/s10973-016-5281-5.

11) M. Chandrashekara, and A. Yadav, "Experimental study of exfoliated graphite solar thermal coating on a receiver with a scheffler dish and latent heat storage for desalination," Solar Energy, 151 129–145 (2017). doi:10.1016/j.solener.2017.05.027.
12) N. Mehla, and A. Yadav, "Experimental analysis of thermal performance of evacuated tube solar air collector with phase change material for sunshine and off-sunshine hours," International Journal of Ambient Energy, 38 (2) 130–145 (2017). doi:10.1080/01430750.2015.1074612.
13) N. Mehla, and A. Yadav, "Thermal analysis on charging and discharging behaviour of a phase change material-based evacuated tube solar air collector," Indoor and Built Environment, 27 (2) 156–172 (2018). doi:10.1177/1420326X16667626.
14) U. Kumar, H. Agrawal, M. Chandrashekara, and A. Yadav, "Fabrication of portable solar thermal bank for indoor cooking," Heat Transfer, 51 (5) 3815–3829 (2022). doi:10.1002/htj.22478.
15) D. Buddhi, and L.K. Sahoo, "Solar cooker with latent heat storage: design and experimental testing," Energy Convers Manag, 38 (5) 493–498 (1997). doi:10.1016/S0196-8904(96)00066-0.
16) C.R. Chen, A. Sharma, S.K. Tyagi, and D. Buddhi, "Numerical heat transfer studies of pcms used in a box-type solar cooker," Renew Energy, 33 (5) 1121–1129 (2008). doi:10.1016/J.RENENE.2007.06.014.
17) R.E. Murray, and D. Groulx, "Experimental study of the phase change and energy characteristics inside a cylindrical latent heat energy storage system: part 2 simultaneous charging and discharging," Renew Energy, 63 724–734 (2014). doi:10.1016/J.RENENE.2013.10.004.
18) G.S. Sodhi, A.K. Jaiswal, K. Vigneshwaran, and P. Muthukumar, "Investigation of charging and discharging characteristics of a horizontal conical shell and tube latent thermal energy storage device," Energy Convers Manag, 188 381–397 (2019). doi:10.1016/J.ENCONMAN.2019.03.022.
19) E.B.S. Mettawee, and G.M.R. Assassa, "Thermal conductivity enhancement in a latent heat storage system," Solar Energy, 81 (7) 839–845 (2007). doi:10.1016/J.SOLENER.2006.11.009.
20) P. Byrne, N. Putra, T. Maré, N. Abdallah, P. Lalanne, I. Alhamid, P. Estelle, A. Yatim, and A.L. Tiffonnet, "Design of a solar ac system including a pcm storage for sustainable resorts in tropical region," Evergreen, 6 (2) 143–148 (2019). doi:10.5109/2321009.
21) D.G. Gunjo, V.K. Yadav, and D.K. Sinha, "Performance analysis of latent heat storage systems using cuo nanoparticles," Evergreen, 9 (2) 292–299 (2022). doi:10.5109/4793667.
22) A.R. Karimi, M. Siavashi, M. Tahmasbi, and A.M. Norouzi, "Experimental analysis to improve charge/discharge of thermal energy storage in phase change materials using helical coil and porous metal foam," J Energy Storage, 55 105759 (2022). doi:10.1016/J.EST.2022.105759.
23) F. Agyenim, P. Eames, and M. Smyth, "Heat transfer enhancement in medium temperature thermal energy storage system using a multitube heat transfer array," Renew Energy, 35 (1) 198–207 (2010). doi:10.1016/J.RENENE.2009.03.010.
24) Y. Zhang, B. Lu, Z. Wang, J. Zhu, J. Zhang, and C. Wang, "Experimental investigation on the charging and discharging performance enhancement of a vertical latent heat thermal energy storage unit via snowflake fin design," Int J Heat Mass Transf, 199 123455 (2022). doi:10.1016/J.IJHEATMASSTRANSFER.2022.123455.
25) M. Lacroix, "Study of the heat transfer behavior of a latent heat thermal energy storage unit with a finned tube," Int J Heat Mass Transf, 36 (8) 2083–2092 (1993). doi:10.1016/S0017-9310(05)80139-5.
26) B.M.S. Punniakodi, and R. Senthil, "Experimental study on melting enhancement of phase change material in a vertical cylindrical latent heat storage using a short concentric helical heat transfer tube," J Energy Storage, 41 102879 (2021). doi:10.1016/J.EST.2021.102879.
27) R. Velraj, R. v. Seeniraj, B. Hafner, C. Faber, and K. Schwarzer, "Experimental analysis and numerical modelling of inward solidification on a finned vertical tube for a latent heat storage unit," Solar Energy, 60 (5) 281–290 (1997). doi:10.1016/S0038-092X(96)00167-3.
28) B. v. Rudra Murthy, K. Thanaiah, and V. Gumtapure, "Experimental investigation of shellac wax as potential bio-phase change material for medium temperature solar thermal energy storage applications," Solar Energy, 231 1002–1014 (2022). doi:10.1016/j.solener.2021.12.019.
29) C. Liu, and D. Groulx, "Experimental study of the phase change heat transfer inside a horizontal cylindrical latent heat energy storage system," International Journal of Thermal Sciences, 82 (1) 100–110 (2014). doi:10.1016/J.IJTHERMALSCI.2014.03.014.
30) M.K. Rathod, and J. Banerjee, "Experimental investigations on latent heat storage unit using paraffin wax as phase change material," Experimental Heat Transfer, 27 (1) 40–55 (2014). doi:10.1080/08916152.2012.719065.
31) M.K. Rathod, and J. Banerjee, "Thermal performance enhancement of shell and tube latent heat storage unit using longitudinal fins," Appl Therm Eng, 75 1084–1092 (2015). doi:10.1016/J.APPLTHERMALENG.2014.10.074.
32) N.R. Vyshak, and G. Jilani, "Numerical analysis of latent heat thermal energy storage system," Energy Convers Manag, 48 (7) 2161–2168 (2007). doi:10.1016/J.ENCONMAN.2006.12.013.

33) M.J. Hosseini, A.A. Ranjbar, K. Sedighi, and M. Rahimi, "A combined experimental and computational study on the melting behavior of a medium temperature phase change storage material inside shell and tube heat exchanger," International Communications in Heat and Mass Transfer, 39 (9) 1416–1424 (2012). doi:10.1016/J.ICHEATMASSTRANSFER.2012.07.028.
34) P.D. Silva, L.C. Gonçalves, and L. Pires, "Transient behaviour of a latent-heat thermal-energy store: numerical and experimental studies," Appl Energy, 73 (1) 83–98 (2002). doi:10.1016/S0306-2619(02)00060-0.
35) Z. Khan, and Z.A. Khan, "Experimental investigations of charging/melting cycles of paraffin in a novel shell and tube with longitudinal fins based heat storage design solution for domestic and industrial applications," Appl Energy, 206 1158–1168 (2017). doi:10.1016/J.APENERGY.2017.10.043.
36) Z. Khan, and Z.A. Khan, "Thermodynamic performance of a novel shell-and-tube heat exchanger incorporating paraffin as thermal storage solution for domestic and commercial applications," Appl Therm Eng, 160 (2019). doi:10.1016/j.applthermaleng.2019.114007.
37) B. Zivkovic, and I. Fujii, "An analysis of isothermal phase change of phase change material within rectangular and cylindrical containers," Solar Energy, 70 (1) 51–61 (2001). doi:10.1016/S0038-092X(00)00112-2.
38) P.H. Biwole, D. Groulx, F. Souayfane, and T. Chiu, "Influence of fin size and distribution on solid-liquid phase change in a rectangular enclosure," International Journal of Thermal Sciences, 124 433–446 (2018). doi:10.1016/J.IJTHERMALSCI.2017.10.038.
39) P. Lamberg, and K. Sirén, "Analytical model for melting in a semi-infinite pcm storage with an internal fin," Heat and Mass Transfer/Waerme- Und Stoffuebertragung, 39 (2) 167–176 (2003). doi:10.1007/s00231-002-0291-1.
40) V. Kumar, and A. Yadav, "Development and thermal performance evaluation of solar parabolic dish based on fiber-reinforced plastic," Heat Transfer, 51 (7) 6222–6248 (2022). doi:10.1002/HTJ.22589.